PROCEEDINGS OF SPIE

SPIEDigitalLibrary.org/conference-proceedings-of-spie

Highly dense FBG arrays for millimeter-scale thermal monitoring during nanocomposite-enhanced laser ablation

Korganbayev, Sanzhar, Asadi, Somayeh, Wolf, Alexey, Dostovalov, Alexander, Zalteri, Martina, et al.

Sanzhar Korganbayev, Somayeh Asadi, Alexey Wolf, Alexander Dostovalov, Martina Zalteri, Emiliano Schena, Haim Azhari, Iris Sonia Weitz, Paola Saccomandi, "Highly dense FBG arrays for millimeter-scale thermal monitoring during nanocomposite-enhanced laser ablation," Proc. SPIE 11354, Optical Sensing and Detection VI, 113540G (1 April 2020); doi: 10.1117/12.2555436

SPIE.

Event: SPIE Photonics Europe, 2020, Online Only, France

Highly dense FBG arrays for millimeter-scale thermal monitoring during nanocomposite-enhanced laser ablation

Sanzhar Korganbayev*[a], Somayeh Asadi[a], Alexey Wolf[b], Alexander Dostovalov[b], Martina Zaltieri[c], Emiliano Schena[c], Haim Azhari[d], Iris Sonia Weitz[e], Paola Saccomandi[a]
[a]Department of Mechanical Engineering, Politecnico di Milano, 1 Via Giuseppe La Masa, 20156 Milano, Italy; [b]Laboratory of Fiber Optics, Institute of Automation and Electrometry SB RAS, Novosibirsk, Russia; [c]Measurements and Biomedical Instrumentation Lab, Università Campus Bio-Medico di Roma, Via Alvaro del Portillo, 21-00128 Rome, Italy; [d]Department of Biomedical Eng. Technion, Israel Institute of Technology, Haifa, Israel; [e]Department of Biotechnology Engineering, ORT Braude College, 2161002 Karmiel, Israel

ABSTRACT

In this study, we assess the feasibility of highly dense fiber Bragg grating (FBG) arrays for real-time temperature measurement during Nanocomposites (NCs)-enhanced laser ablation (LA) of pancreas tissue. FBG arrays were fabricated with the femtosecond point-by-point writing technology. Each highly dense array contains 25 FBGs with a grating length of 0.9 mm and an edge-to-edge distance of 0.1 mm. As alternative fiber sensors, we used commercially available acrylate-coated FBG arrays containing 5 FBGs. Temperature measurements by the highly dense FBG array were compared to thermal camera readings during laser irradiation of water samples. The augmented thermal effect produced by special NC comprising of a polydopamine matrix embedded with gold and copper was evaluated during the irradiation of an *ex vivo* phantom. The phantom consisted of a blended porcine pancreas tissue mixed with the NC; tissue mixed with water was used for control. The results clearly demonstrate that the highly dense arrays better detect the peak temperature and temperature distribution. The NC presence increased the maximum temperature reached during LA from 48 °C (control) to 90 °C (NC) at 2 mm, and from 33 °C to 36 °C at 4 mm distance from the laser tip. The low spatial resolution of the commercial arrays produced an underestimation of the peak temperature by 2 °C (control), and by 1 °C (NC) at 4 mm. These results highlight the importance of the proper selection of the measurement system characteristics, especially when high temperature gradient should be measured in biological tissues undergoing thermal ablation for cancer treatment.

Keywords: pancreas cancer, thermal ablation, laser ablation, Au/Cu-polydopamine, fiber sensor, fiber Bragg grating.

1. INTRODUCTION

Thermal treatments of solid tumors are becoming more and more popular as an alternative to traditional surgical methods. This stems from their minimal invasive nature when conducted with endoscopic applicators under percutaneous guidance, and their lower collateral damage to healthy tissues [1], [2]. Depending on the energy source used for the treatment, they are divided into: microwave [3], radiofrequency [4], high-intensity focused ultrasound [5], laser ablations [7] and cryoablation [6]. During all treatments the temperature is increased slightly above the cytotoxic level (50 – 60 °C) [8], except for cryoablation, where the tumor is destroyed freezing the tissue [9]. Among these methods, LA is particularly attractive due to its MRI-compatibility and the possibility to use small flexible fiber to guide laser energy into deep-lying tumors [7]. Laser energy absorption and its transformation to heat near the applicator's tip leads to tumor cell death during LA. LA has been used for prostate, liver, kidney, lung [10], and pancreas [11], [12]. Despite the abovementioned advantages, LA can still present incomplete ablation and disease recurrence due to the low selectivity of laser light with respect to the tumor tissue, hence leading to possible damage to surrounding healthy tissues. These limitations can significantly decrease the efficacy of the treatment [13].

In order to solve this problem, nanoparticle (NP)-enhanced laser ablation was proposed to localize the heat increase in the tumor: specifically designed NPs that highly absorb laser light are injected in the tumor tissue [14]. As a result, the temperature is increased only in the confined tumor volume. In order to evaluate the effect of NPs during *in vitro, ex vivo*

*sanzhar.korganbayev@polimi.it

Optical Sensing and Detection VI, edited by Francis Berghmans, Anna G. Mignani, Proc. of SPIE
Vol. 11354, 113540G · © 2020 SPIE · CCC code: 0277-786X/20/$21 · doi: 10.1117/12.2555436

and, in rare cases, *in vivo* studies, different experimental setups were used: infrared thermal camera [15]–[17], thermocouples [18], [19], multifunctional luminescent nanothermometers capable of simultaneous heating and thermal sensing [15], [20]. All these methods have some disadvantages: thermocouples are not MRI compatible and can provide only point measurements; thermal camera provides superficial measurement; and most of nanothermometers operate in the visible spectrum domain, where optical penetration into tissues is minimal [15], [21].

In this work we suggest the use of fiber Bragg grating (FBG) arrays for evaluating the thermal effect stemming from the presence of NCs made by polydopamine matrix embedded with the gold NPs and copper species (Au/Cu@PDA). FBG arrays, as most of optical fiber sensors, are immune to electromagnetic interference, small (40-250 μm diameter) and biocompatible. Also, FBG arrays allow quasi-distributed temperature and strain sensing across the fiber [22], [23]. The effect was assessed during irradiation of the *ex vivo* phantom consisted of blended porcine pancreas tissue mixed with the NCs.

2. METHODS

2.1 Fiber Bragg grating sensing

For temperature measurements during LA, we used fiber optic sensors based on the FBG phenomenon. An FBG is a wavelength-dependent reflector resulting from a periodic variation of the refractive index in the fiber core: it reflects only a specific wavelength while transmitting others. The reflected wavelength, λ_B, is proportional to the grating period Λ (distance between two regions with high refractive indices) [24]:

$$\lambda_B = 2n_{eff}\Lambda \tag{1}$$

Temperature or strain applied to an FBG changes the grating period Λ, that, in his turn, alters λ_B. Under constant strain conditions, the measurement of this Bragg shift, $\Delta\lambda_B$, can be used to reconstruct temperature change, ΔT , applied to the grating, making each FBG to be a temperature point sensor:

$$\Delta\lambda_B = \lambda_{B,\Delta T} - \lambda_{B,initial} = k\Delta T \tag{2}$$

where k [nm/°C] is the thermal sensitivity of the grating.

It is possible to inscribe a chain of FBGs with different grating periods in one fiber. This chain, also called an FBG array, reflects a set of different λ_B, analysis of which allows multi-point temperature measurement across the fiber.

For our experiments, we used highly dense FBG arrays inscribed in a special polyimide-coated single-mode optical fiber using the femtosecond point-by-point writing technology [25]. Polyimide coating provides higher temperature resistance (short term up to 400 °C and continuous operation at 300 °C) in comparison with acrylate one (up to 85 °C) [25], [26]. Each array has 25 FBGs with a 0.9 mm grating length and a 0.1 mm edge-to-edge distance between gratings. In order to have a wavelength-division multiplexing of the array (to discriminate FBGs in the spectral region) the periods of the gratings and related Bragg wavelengths were changed along the array. Fig.1a depicts the reflection spectrum of the array measured by the Micron Optics si255 interrogation unit (*Micron Optics*, Atlanta, USA). Temperature sensitivity coefficients of the FBG arrays were obtained after the calibration in a thermal chamber for 30 °C to 140 °C temperature range. As alternative sensors, we used commercially available acrylate-coated FBG arrays containing 5 FBGs with 1 mm grating length and 2 mm edge-to-edge spacing (*AtGrating Technologies*, Shenzhen, China).

2.2 Preparation of gold/copper–polydopamine nanocomposite

NC consisting of mussel-inspired polydopamine (PDA), gold NPs and copper species, was prepared by *in situ* co-reduction approach as described in our recently published work [27]. First, the precursor of copper oxide NPs was loaded during oxidative polymerization of dopamine in the presence of air and Tris buffer (pH 8.5). Then, the acidic solution of $HAuCl_4$ was added to initiate a redox reactions between the PDA and metal ions (Au^{3+} and Cu^{2+}). As a result, water soluble Au/Cu@PDA NC was formed. Cryogenic transmission electron microscopy (cryo-TEM, FEI Talos 200C) was used to visualize the presence of the gold NPs embedded in the PDA matrix, the two components that mainly provide the photothermal behavior (Fig. 1b).

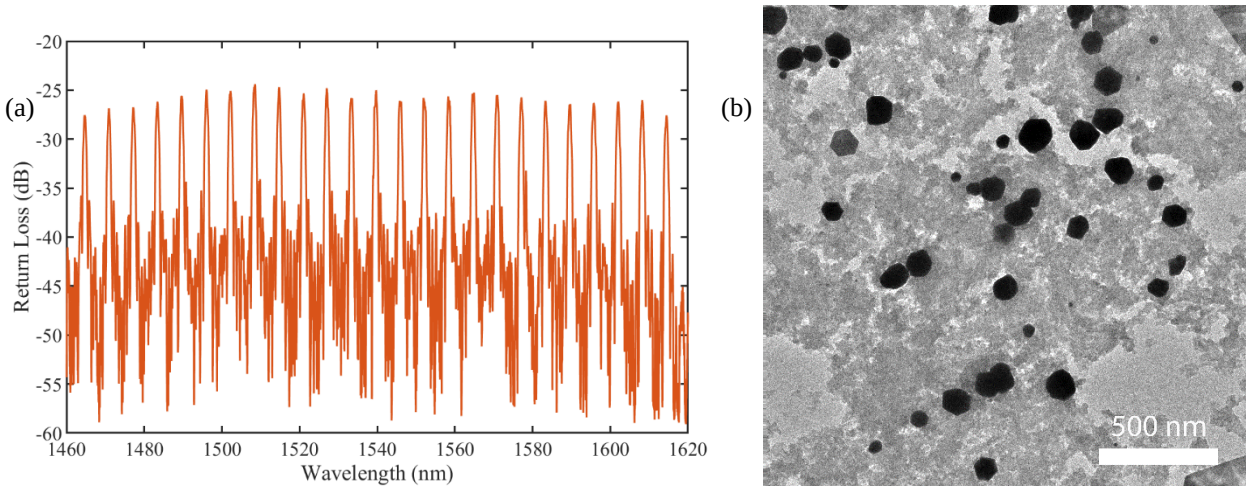

Figure 1. (a) Reflection spectrum of the fabricated highly dense FBG array with the femtosecond point-by-point writing technology: 25 peak Bragg reflections equidistant in 1464.5-1614.5 nm wavelength range; (b) Cryo-TEM image of Au/Cu@PDA nanocomposite (scale bar is 500 nm).

2.3 Experimental setup

The main experimental setup is shown in Fig. 2: continuous wave (CW) LA was performed by a diode laser LuOcean Mini 4 (Lumics GmbH, Berlin, Germany) with a wavelength of λ=808 nm, an output power of 2.2 W and a treatment time of 10 s guided by a 300 μm-diameter quartz optical fiber immersed in the *ex vivo* phantom placed in a 1.5 ml quartz cuvette. The phantom consisted of blended porcine pancreas tissue mixed with the PDA NCs embedded with gold NPs and copper species; tissue mixed with water was used for control measurements. The laser-guiding fiber and arrays were immersed in the phantom parallel to each other, and LA was repeated three times. FBG arrays were positioned at fixed distances (2 mm and 4 mm) from the applicator tip. The acrylate-coated FBG array with 5 gratings was not placed at 2 mm distance in order to prevent possible damage of the fiber due to high temperatures. Spectra measured during ablation were analyzed to reconstruct temperature profiles across the FBG arrays.

Also, a comparison of the highly dense FBG array and the thermal camera measurements was done during the laser irradiation of a distilled water in the cuvette. In this case, only one array of 25 FBGs was positioned at a 2 mm distance from the laser tip. The infrared thermal imaging camera (FLIR T540, FLIR® Systems, Inc), positioned at a 30 cm distance, measured the surface temperature of the cuvette walls at a 10 Hz rate.

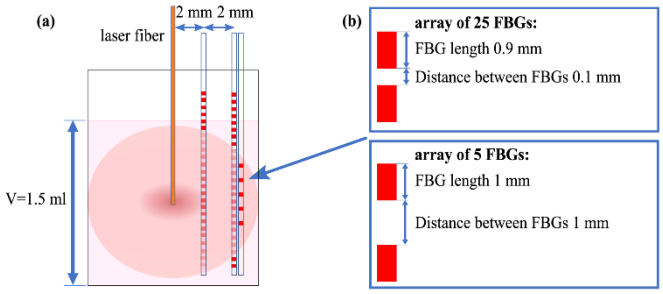

Figure 2. (a) Schematic representation of the laser ablation of the porcine phantom placed in quartz cuvette: FBG arrays were positioned at 2 mm (the highly dense array) and 4 mm (the highly dense array and the acrylate-coated FBG array with 5 gratings) from the applicator tip; (b) Zoom-in of the schematic illustrating dimension characteristics of the gratings.

3. EXPERIMENTAL RESULTS

3.1 The highly dense FBG array and the infrared thermal camera measurements comparison

For this experiment, the temperature during laser irradiation of water in the quartz cuvette was measured with the FBG arrays and the thermal camera. Both techniques were not able to measure the real maximum temperature of the water because the FBG arrays were positioned at 2 mm distance from the tip, while the camera measured only the surface temperature of the cuvette walls. Fig. 3a reports the highest temperatures measured by both techniques during the irradiation. As can be seen, the camera significantly underestimates the maximum temperature of the solution as it measures the temperature of the walls. Moreover, this underestimation can be even higher in the case of confined temperature increase near the laser tip (for example, during irradiation of the solution with lower heat conduction to the cuvette walls).

3.2 The effect of the NCs presence during laser irradiation of the pancreas phantom

Fig. 3b illustrates peak temperature profiles measured during the laser irradiation. The NCs (Au/CuO@PDA) presence increased the maximum temperature reached during LA from 48 °C (control) to 90 °C (NCs) at 2 mm. While at 4 mm distance, the NCs presence increased temperature from 33 °C to 36 °C (measured by 25 FBGs), and from 31 °C to 35 °C (measured by 5 FBGs). The low spatial resolution of the commercial arrays produced an underestimation (in comparison with the highly dense arrays) of the peak temperature by 2 °C (control), and by 1 °C (NCs) at 4 mm.

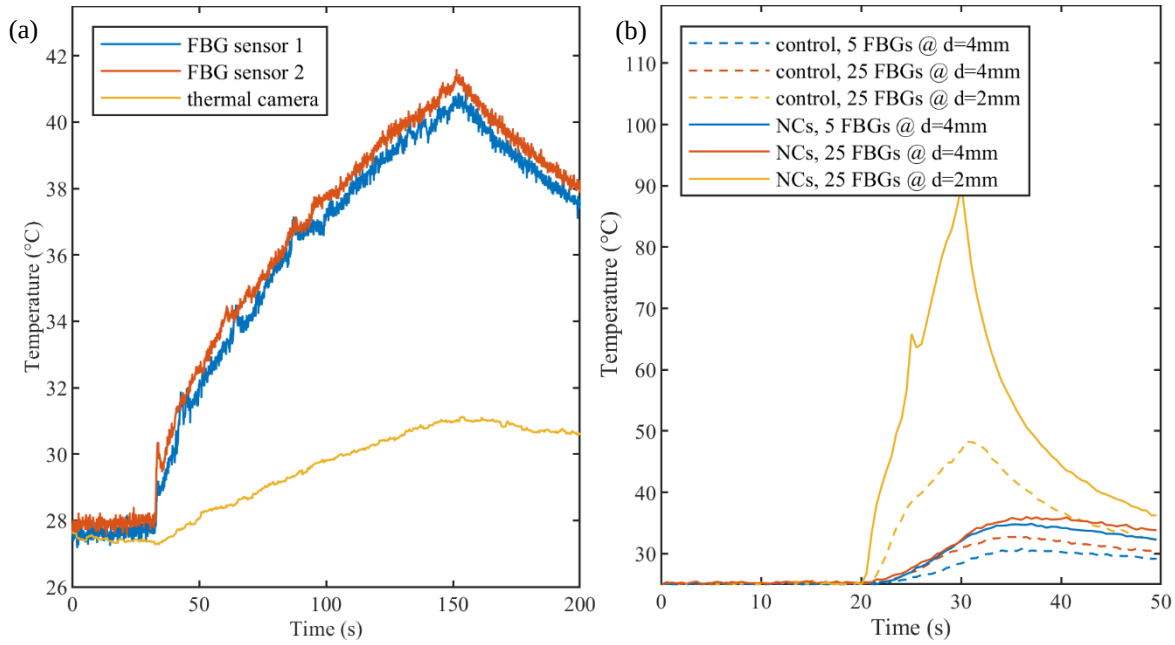

Figure 3. (a) The maximum temperatures of the solution in cuvette measured by the FBG sensors and the thermal camera; (b) peak temperature profiles measured during laser ablation of the control sample (pancreas tissue mixed with water) and experimental one (pancreas tissue mixed with the PDA NC embedded with gold NPs and copper species). The array with 5 FBGs (blue color) underestimates the maximum temperature due to the lower resolution of the array.

Fig. 4 reports thermal maps (distance along the sensor *vs* time) during the laser irradiation of the experimental sample measured by the commercial and the highly dense arrays at a 4 mm distance from the applicator tip. After the irradiation starts at 20 s, the temperature increases, and the heat distributes towards the edges of the sensing length of the array. When ablation is over, the temperature starts to decrease, but the heat dissipation is continuing towards the edges. The highly dense array in comparison with the commercial one has a higher spatial resolution (1 mm *vs* 2 mm) and longer sensing length (25 mm *vs* 9 mm), that results in better thermal maps.

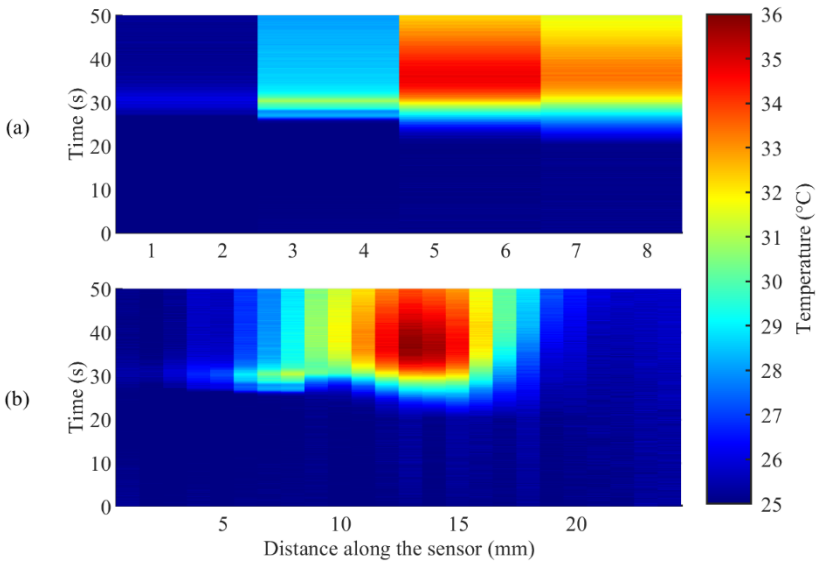

Figure 4. Two-dimensional thermal maps (distance along the sensor *vs* time) during laser irradiation of the pancreas tissue blended with NCs at a 4 mm distance measured by: (a) the commercial array with 5 FBGs; (b) the highly dense array with 25 FBGs.

4. CONCLUSION AND DISCUSSIONS

This work presents the evaluation and feasibility of highly dense FBG arrays for thermal measurements during *in vitro* laser irradiations. We used the femtosecond point-by-point writing technology to inscribe the FBG array with high spatial resolution properties, resulting in a 0.9 mm grating length and an edge-to-edge distance of 0.1 mm. As alternative sensors, commercially available acrylate-coated FBG arrays with 5 FBGs and thermal imaging camera were used. We used the FBG arrays to evaluate the effect stemming from the presence of polydopamine matrix embedded with gold NPs and copper species in *ex vivo* phantom consisted of blended porcine during laser irradiation of the sample.

The presence of the NCs in the sample resulted in an increase of the maximum temperature reached during LA from 33 °C to 36 °C at 4 mm, and from 48 °C (control) to 90 °C (NCs) at 2 mm distance from the laser tip. The commercial array measurements produced an underestimation (in comparison with the highly dense arrays) of the peak temperature by 2 °C (control), and by 1 °C (NCs) at 4 mm. The obtained thermal maps clearly show that longer sensing length and better resolution of the highly dense arrays result in more accurate information about heat distribution in the sample.

The results show that the proposed use of FBG array for controlled ablation provides several advantages over thermal measurements with thermocouples, thermistors and infrared cameras [15]–[19]. Highly dense multi-point temperature sensing capability of FBG array provides more accurate peak temperature detection and measurement of spatial heat distribution during laser ablation. Also, FBG arrays are minimally invasive, biocompatible, and immune to electromagnetic interference. These qualities make them well suited for cancer thermal treatments. The results of this study encourage further applications of highly dense fiber Bragg arrays for evaluation of the thermal maps near the laser applicator during laser irradiation in laser ablation during *in vitro* and *ex vivo* studies.

ACKNOWLEDGMENTS

The authors are grateful to Dr. Ellina Kesselman and Dr. Na'ama Koifman for TEM imaging (Technion Center for Electron Microscopy of Soft Matter (TCEMSM)), and thank Inbal Maor and Neta Abarbanel for their technical assistance.

This project has received funding from the European Research Council (ERC) under the European Union's Horizon 2020 research and innovation program (GA n. 759159).

REFERENCES

[1] K. F. Chu and D. E. Dupuy, "Thermal ablation of tumours: biological mechanisms and advances in therapy," *Nat. Rev. Cancer*, vol. 14, no. 3, p. 199, 2014.

[2] M. Ahmed, C. L. Brace, F. T. Lee Jr, and S. N. Goldberg, "Principles of and advances in percutaneous ablation," *Radiology*, vol. 258, no. 2, pp. 351–369, 2011.

[3] M. G. Lubner, C. L. Brace, J. L. Hinshaw, and F. T. Lee Jr, "Microwave tumor ablation: mechanism of action, clinical results, and devices," *J. Vasc. Interv. Radiol.*, vol. 21, no. 8, pp. S192–S203, 2010.

[4] S. N. Goldberg, "Radiofrequency tumor ablation: principles and techniques," in *Multi-Treatment Modalities of Liver Tumours*, Springer, 2002, pp. 87–118.

[5] Y.-F. Zhou, "High intensity focused ultrasound in clinical tumor ablation," *World J. Clin. Oncol.*, 2011, doi: 10.5306/wjco.v2.i1.8.

[6] S. Tatli, M. Acar, K. Tuncali, P. R. Morrison, and S. Silverman, "Percutaneous cryoablation techniques and clinical applications," *Diagnostic Interv. Radiol.*, vol. 16, no. 1, p. 90, 2010.

[7] E. Schena, P. Saccomandi, and Y. Fong, "Laser Ablation for Cancer: Past, Present and Future," *J. Funct. Biomater.*, 2017, doi: 10.3390/jfb8020019.

[8] C. L. Brace, "Radiofrequency and microwave ablation of the liver, lung, kidney, and bone: what are the differences?," *Curr. Probl. Diagn. Radiol.*, vol. 38, no. 3, pp. 135–143, 2009.

[9] M. Shafir, R. Shapiro, M. Sung, R. Warner, A. Sicular, and A. Klipfei, "Cryoablation of unresectable malignant liver tumors," *Am. J. Surg.*, vol. 171, no. 1, pp. 27–31, 1996.

[10] G. J. Müller and A. Roggan, *Laser-induced interstitial thermotherapy*. SPIE Press, 1995.

[11] F. Di Matteo *et al.*, "EUS-guided Nd: YAG laser ablation of normal pancreatic tissue: a pilot study in a pig model," *Gastrointest. Endosc.*, vol. 72, no. 2, pp. 358–363, 2010.

[12] P. Saccomandi *et al.*, "Laser Interstitial Thermotherapy for pancreatic tumor ablation: Theoretical model and experimental validation," in *Proceedings of the Annual International Conference of the IEEE Engineering in Medicine and Biology Society, EMBS*, 2011, doi: 10.1109/IEMBS.2011.6091351.

[13] E. Schena, P. Saccomandi, and Y. Fong, "Laser Ablation for Cancer: Past, Present and Future," *J. Funct. Biomater.*, vol. 8, no. 2, p. 19, 2017, doi: 10.3390/jfb8020019.

[14] R. Mooney, E. Schena, P. Saccomandi, A. Zhumkhawala, K. Aboody, and J. M. Berlin, "Gold nanorod-mediated near-infrared laser ablation: in vivo experiments on mice and theoretical analysis at different settings," *Int. J. Hyperth.*, 2017, doi: 10.1080/02656736.2016.1230682.

[15] E. C. Ximendes, U. Rocha, K. U. Kumar, C. Jacinto, and D. Jaque, "LaF3 core/shell nanoparticles for subcutaneous heating and thermal sensing in the second biological-window," *Appl. Phys. Lett.*, vol. 108, no. 25, p. 253103, 2016.

[16] M. Li *et al.*, "NIR-Activated Polydopamine-Coated Carrier-Free 'Nanobomb' for In Situ On-Demand Drug Release," *Adv. Sci.*, vol. 5, no. 7, p. 1800155, 2018.

[17] S. J. Ashrafi, F. Yazdian, A. S. H. Zaremi, J. Mohhamadnejad, and R. Dinarvand, "Thermal Distribution of Silica Coated Gold Nano Rods in Tissue-Like Phantom as In Vitro Model for Plasmonic Photo Thermal Therapy.," *Biomed. Pharmacol. J.*, vol. 9, no. 3, pp. 1189–1201, 2016.

[18] D. Cassano, M. Santi, F. D'Autilia, A. K. Mapanao, S. Luin, and V. Voliani, "Photothermal effect by NIR-responsive excretable ultrasmall-in-nano architectures," *Mater. Horizons*, vol. 6, no. 3, pp. 531–537, 2019, doi: 10.1039/c9mh00096h.

[19] J. T. Lin, Y. S. Chiang, G. H. Lin, H. Lee, and H. W. Liu, "In vitro photothermal destruction of cancer cells using gold nanorods and pulsed-train near-infrared laser," *J. Nanomater.*, vol. 2012, 2012, doi: 10.1155/2012/861385.

[20] E. C. Ximendes *et al.*, "Unveiling in vivo subcutaneous thermal dynamics by infrared luminescent nanothermometers," *Nano Lett.*, vol. 16, no. 3, pp. 1695–1703, 2016.

[21] P. Saccomandi, E. Schena, and S. Silvestri, "Techniques for temperature monitoring during laser-induced thermotherapy: An overview," *Int. J. Hyperth.*, vol. 29, no. 7, pp. 609–619, 2013, doi: 10.3109/02656736.2013.832411.

[22] A. Othonos, K. Kalli, and G. E. Kohnke, "Fiber Bragg gratings: Fundamentals and applications in telecommunications and sensing," *Phys. Today*, vol. 53, no. 5, p. 61, 2000.

[23] E. Udd and W. B. Spillman Jr, *Fiber optic sensors: an introduction for engineers and scientists*. John Wiley & Sons, 2011.

[24] T. Erdogan, “Fiber grating spectra,” *J. Light. Technol.*, vol. 15, no. 8, pp. 1277–1294, 1997.
[25] A. V Dostovalov, A. A. Wolf, A. V Parygin, V. E. Zyubin, and S. A. Babin, “Femtosecond point-by-point inscription of Bragg gratings by drawing a coated fiber through ferrule,” *Opt. Express*, vol. 24, no. 15, pp. 16232–16237, 2016.
[26] K. T. V Gratten and B. T. Meggitt, *Optical Fiber Sensor Technology: Volume 3: Applications and Systems*, vol. 3. Kluwer Academic Pub, 1999.
[27] O. Perlman, A. Borodetsky, Y. Kauffmann, Y. Shamay, H. Azhari, and I. S. Weitz, “Gold/Copper@ Polydopamine Nanocomposite for Contrast-Enhanced Dual Modal Computed Tomography–Magnetic Resonance Imaging,” *ACS Appl. Nano Mater.*, vol. 2, no. 10, pp. 6124–6134, 2019.